Theor Ecol (2018) 11:55–69
https://doi.org/10.1007/s12080-017-0348-x

ORIGINAL PAPER

The dispersal success and persistence of populations with asymmetric dispersal

D. Scott Rinnan[1]

Received: 14 February 2017 / Accepted: 6 October 2017 / Published online: 16 October 2017

Abstract Asymmetric dispersal is a common trait among populations, often attributed to heterogeneity and stochasticity in both environment and demography. The cumulative effects of population dispersal in space and time have been described with some success by Van Kirk and Lewis's average dispersal success approximation (Bull Math Biol 59(1): 107–137 1997), but this approximation has been demonstrated to perform poorly when applied to asymmetric dispersal. Here we provide a comparison of different characterizations of dispersal success and demonstrate how to capture the effects of asymmetric dispersal. We apply these different methods to a variety of integrodifference equation population models with asymmetric dispersal, and examine the methods' effectiveness in approximating key ecological traits of the models, such as the critical patch size and the critical speed of climate change for population persistence.

Keywords Average dispersal success · Asymmetric dispersal · Integrodifference equation · Moving habitat model · Population persistence · Climate change

Introduction

Dispersal—defined by Trakhtenbrot et al. (2005) as the movement of organisms, their propagules, or their genes away from the source population—can have a profound effect on the persistence and spread of populations through space and time. Spatial population models commonly describe the dispersal process by means of a dispersal kernel $k(x, y)$, a probability density function that reflects the likelihood of moving from the location y to the point x in a single time step. Dispersal kernels have been derived from observations of dispersal events for a variety of populations and species, including trees (Clark et al. 1999; Nathan and Muller-Landau 2000), plants (Willson 1993), birds (Veit and Lewis 1996), and fish (Rodríguez 2010). Dispersal is often represented as a symmetric process, under the assumption that dispersal in any direction is equally likely (Vuilleumier and Possingham 2006).

A clear and consistent pattern throughout the literature, however, suggests that biological dispersal is a fundamentally *asymmetric* spatial process: asymmetric dispersal due to wind patterns have been observed in fungal pathogens (Rieux et al. 2014), lichen spores (Werth et al. 2006), and tree pollen (Austerlitz et al. 2007); ocean currents play a similar role in affecting the dispersal of marine organisms (Byers and Pringle 2006), and stream currents for aquatic insects (Lutscher et al. 2010); population persistence in a habitat shifting due to climate change can be characterized by asymmetric dispersal (Zhou and Kot 2011; Bouhours and Lewis 2016); elevational asymmetries in dispersal have been observed in a variety of montane habitats (Willson and Traveset 2000). Indeed, asymmetric dispersal seems to be the rule rather than the exception. Although many researchers readily acknowledge the significance of the possible effects of asymmetric dispersal, it appears uncommon for asymmetric dispersal to be explicitly incorporated into spatial population models, likely due to the mathematical complexity involved, or a simple lack of data.

The concept of *average dispersal success* (ADS) has proven to be a useful tool for addressing many of the issues that arise from a scarcity of dispersal data and model complexity.

✉ D. Scott Rinnan
rinnan@u.washington.edu

[1] Quantitative Ecology and Resource Management, University of Washington, Box 357941, Seattle, WA 98195-7941, USA

Van Kirk and Lewis (1997) defined a population's average dispersal success S across a patch of habitat Ω as

$$S = \frac{1}{\Omega} \int_{\Omega} \int_{\Omega} k(x, y)\, dx\, dy, \tag{1}$$

the spatially averaged probability of remaining in Ω after dispersal, assuming that the individual begins in Ω. Alternatively, this can be interpreted as the proportion of individuals beginning in Ω that remain in Ω after dispersing. ADS distinguishes individuals that disperse "locally" (i.e., within the habitat patch) from those that disperse "farther away" (i.e., outside the habitat patch), and in doing so, provides a tool for relating field data collected at a regional scale to population dynamics at a larger scale (Fagan and Lutscher 2006). Dispersal success has been used to address a variety of questions in conservation ecology such as reserve network design in marine systems (Baskett et al. 2007), metapopulation dynamics (Fagan and Lutscher 2006), and population dynamics of caterpillars (Hughes et al. 2015) and stream insects (Vasilyeva et al. 2016).

As defined in Eq. 1, however, ADS has its limitations. In particular, Van Kirk and Lewis (1997) explored S only in the context of symmetric dispersal. Although they suggested a method for generalizing S to asymmetric kernels, this method has nonetheless been shown to provide an increasingly poor approximation of the effects of dispersal for increasingly asymmetric kernels (Reimer et al. 2016). This limitation is unfortunate, because a great deal of insight might be gleaned from studying the consequences of asymmetric dispersal, and, given the aforementioned ubiquity of the phenomenon, an accurate, generalizable method that quantifies asymmetric dispersal success would apply to a much a wider variety of ecological processes and issues of considerable current interest.

One such issue is the effect of climate change on population persistence. A large number of species are expected to be unable to keep pace with the speed at which their suitable habitat is shifting due to the effects of climate change (Chen et al. 2011; Schloss et al. 2012). Fewer individuals are able to successfully disperse at higher climate velocities, which leads to fewer individuals that are able to successfully reproduce. In theory, beyond a certain critical speed, the population cannot persist. Zhou and Kot (2011) demonstrated how an asymmetric shifted dispersal kernel can represent the effects of a habitat shifting due to climate change. Another related concept is the threshold of habitat size necessary for persistence. If a population's habitat is too small, individuals cannot reproduce rapidly enough to offset the loss of individuals through dispersal, and the population will eventually die out. Ensuring that the amount of available habitat is sufficient to sustain a population through time is essential for successful reserve design. ADS is ill-suited to address the question of critical climate speed, and can only address critical habitat size if dispersal is assumed to be symmetric.

In this paper, we demonstrate how to adapt ADS to more accurately reflect the consequences of asymmetric dispersal in an integrodifference population model. In Section Persistence criteria and integrodifference equations, we introduce integrodifference equations (IDEs) and discuss their criteria for population persistence. In Section Average dispersal success, we motivate dispersal success in both a mathematical and biological context, and explore (Van Kirk and Lewis 1997)'s original definition S in Eq. 1, and a modification $\widehat{S}$ proposed by Reimer et al. (2016) that weights the integrand of S by population density. In Section Geometric symmetrization, we introduce and formalize the method of geometric symmetrization, a technique that uses a result of linear algebra to address the issue of asymmetric kernels (Kot and Phillips 2015). Finally, in Section Applications to integrodifference models, we apply these three approaches to IDEs with asymmetric dispersal, and explore how each method can be used to estimate the model's critical patch size, critical shift speed, and average population density at equilibrium, and how these estimates compare with one another. The majority of this paper uses shifted kernels to illustrate asymmetric dispersal, but the theory we develop extends to other types of asymmetric kernels as well, which we explictly show in Section Other types of asymmetry.

Persistence criteria and integrodifference equations

The persistence of populations can often be characterized as an eigenvalue problem (Leslie 1945; Caswell 2001). A simple matrix population model, for example, is written as

$$\mathbf{n}_{t+1} = \mathbf{M}\mathbf{n}_t, \tag{2}$$

where $\mathbf{n}_t$ is a vector of population densities of different life stages, and $\mathbf{M}$ is a matrix that describes the rates of transition from one life stage to another. The associated eigenvalue equation of Eq. 2 is

$$\lambda \mathbf{u} = \mathbf{M}\mathbf{u}. \tag{3}$$

Persistence (and growth) of the population will occur when the dominant eigenvalue $\lambda_{\max}$ of $\mathbf{M}$ is greater than 1, and the population will collapse when $\lambda_{\max}$ is less than 1.

Integrodifference equations (IDE), by comparison, use a spatially explicit approach to model a population as

$$N_{t+1}(x) = \int_0^L k(x, y) f[N_t(y)]\, dy, \tag{4}$$

with population $N_t(x)$ at location x and time t, growth function $f[N_t(y)]$, and dispersal kernel $k(x, y)$. Since most

choices of dispersal and growth functions make IDEs analytically intractable, it is not usually possible to obtain an analytic steady-state solution, and we are unaware of any such examples in the literature (although Zhou and Kot 2011 outline a scheme for approximating one example of an IDE with a separable kernel). Instead, various approximation methods are commonly employed. Assuming no Allee effects, and homogeneous and symmetric dispersal such that $k(x, y) = k(|x-y|)$, the corresponding eigenvalue equation of Eq. 4 can be approximated by

$$\lambda u(x) = R_0 \int_0^L k(x-y)u(y)\,dy, \tag{5}$$

with R_0 the net reproductive rate given by $R_0 = f'(0)$, eigenvalue λ and corresponding eigenfunction $u(\bar{x})$ (Kot and Schaffer 1986). Again, the dominant eigenvalue $\lambda_{\max}$ of the integral operator of Eq. 5 determines persistence: for $\lambda_{\max} > 1$, the population will persist, and for $\lambda_{\max} < 1$ the population will die out.

Zhou and Kot (2011) studied the persistence of a population in a habitat shifting in space due to climate change, described by the IDE

$$N_{t+1}(x) = \int_{ct}^{L+ct} k(x, y) f[N_t(y)]\,dy, \tag{6}$$

with associated eigenvalue problem

$$\lambda u(\bar{x}) = R_0 \int_0^L k(\bar{x} + c - \bar{y})u(\bar{y})\,d\bar{y}, \tag{7}$$

where c is the speed of climate change, and $\bar{x} = x - ct$ and $\bar{y} = y - ct$. This equation is an example of the type of eigenvalue problem of primary concern in this paper. An equivalent formulation can be derived from the stationary IDE in Eq. 4 assuming a shifted kernel $k(x+c-y)$, and for other types of asymmetric kernels as we will later see. For the remainder of this paper, we will drop the bars on $\bar{x}$ and $\bar{y}$ for notational convenience when referencing (7).

More recently, Kot and Phillips (2015) explored methods for approximating $\lambda_{\max}$ of Eq. 7, and found that in certain cases,

$$\lambda_{\max} \approx \lambda_S \equiv \frac{R_0}{L} \int_0^L \int_0^L k(x + c - y)\,dx\,dy \tag{8}$$

$$= R_0 S, \tag{9}$$

where S is the average dispersal success in Eq. 1. This reflects a similar approximation (Lutscher and Lewis 2004) derived for stage-structured populations.

To a first-order approximation, Eq. 9 demonstrates how ADS succinctly relates to population persistence: the net reproductive rate must be greater than $1/S$ for the population to persist. We note, however, that our kernel has become asymmetric due to the spatial shift by c. Since we have asserted that S provides a poor approximation in the case of asymmetric dispersal, we might expect λ_S to diverge from the true value of $\lambda_{\max}$ for increasing c, and Kot and Phillips (2015) indeed provide examples in support of our expectations.

We will now provide a brief discussion of ADS, before demonstrating how we can modify it to better capture the effects of asymmetric dispersal.

Average dispersal success

We begin by establishing some basic terminology, following the notational conventions of Van Kirk and Lewis (1997) and Lutscher and Lewis (2004). The *dispersal kernel* $k(x, y)$ is a probability density function that describes the likelihood of an individual dispersing from the location y to the location x by the next time step.

The *dispersal success function* $s(y)$ describes the probability that an individual starting at location y will settle within the domain Ω by the next time step, given by

$$s(y) \equiv \int_\Omega k(x, y)\,dx. \tag{10}$$

Conversely, the *redistribution function* $r(y)$ reflects the probability that an individual starting within the domain Ω will successfully disperse to location y by the next time step, given by

$$r(y) \equiv \int_\Omega k(y, x)\,dx. \tag{11}$$

When the kernel is symmetric we have $k(x, y) = k(y, x)$, and so $r(y) = s(y)$.

Finally, the *average dispersal success* is the spatial average of the dispersal success function, defined by

$$S \equiv \frac{1}{|\Omega|} \int_\Omega s(y)\,dy = \frac{1}{|\Omega|} \int_\Omega \int_\Omega k(x, y)\,dx\,dy, \tag{12}$$

where $|\Omega|$ represents the size of the domain.

The value of S reflects the proportion of a population in Ω that will remain in Ω after a single dispersal event, assuming that the population was initially distributed uniformly throughout Ω. This uniformity is implicit in the fact that all locations in Ω are weighted equally in the spatial average of the dispersal success function $s(y)$ or redistribution function $r(y)$. This naturally invites the question of how to quantify the average dispersal success of a population that is heterogeneously distributed in Ω. Reimer et al. (2016) defined the *modified average dispersal success* $\widehat{S}$, which weighs the dispersal success function by the distribution of individuals in Ω as predicted by $r(y)$, given by

$$\widehat{S} \equiv \frac{1}{|\Omega|} \int_\Omega \frac{r(y)}{S} s(y)\,dy. \tag{13}$$

The value of $\widehat{S}$ reflects the proportion of individuals that will remain in Ω after a single dispersal event, assuming an initial distribution in Ω of $r(y)$.

Under the right conditions, the solution of a population model will converge to an equilibrium. In a spatial population model with symmetric dispersal, this equilibrium often closely resembles $s(y)$ (Van Kirk and Lewis 1997); dispersal success is greatest at the center of Ω and lowest at its edges, and individuals will end up distributed in Ω accordingly. Provided a sufficient growth rate to replenish the proportion of the population that is lost due to dispersal outside Ω, the population stay at this equilibrium indefinitely. As such, when the kernel $k(x, y)$ is symmetric, we may reasonably use S and $\widehat{S}$ to approximate the persistence of a population over time. When $k(x, y)$ is asymmetric, however, individuals disperse with a directional bias, and (by assumption) this bias is persistent through time, affecting each generation equally, and propagating with each successive dispersal event. In this scenario, we might expect that S and $\widehat{S}$ fail to reflect population persistence, since the long-term population equilibrium might be quite different than the population after the first or second dispersal events (Reimer et al. 2016).

Kot and Phillips (2015) described a method for approximating the effects of one such class of asymmetric dispersal kernels, the shifted kernel $k(x, y) = k(x + c - y)$, using geometric symmetrization to construct a symmetric kernel with the same qualitative properties as $k(x, y)$. As we will see, this method can be used to provide a lower bound on the proportion of individuals remaining in Ω at population equilibrium. In the following section, we outline the method, beginning with some relevant results from linear algebra.

Geometric symmetrization

Schwenk (1986) identified a nonnegative, symmetric $m \times m$ matrix $\mathbf{G}$ with dominant eigenvalue $\rho(\mathbf{G})$ that provides a lower bound for the dominant eigenvalue of a nonnegative, asymmetric matrix $\mathbf{A}$. The *geometric symmetrization* $\mathbf{G}$ of $\mathbf{A}$ is defined by the property

$$\mathbf{G} \circ \mathbf{G} = \mathbf{A} \circ \mathbf{A}^T, \tag{14}$$

where $\circ$ is the Hadamard product symbolizing element-wise multiplication, so that element $g_{ij} = g_{ji} = \sqrt{a_{ij}a_{ji}}$ is the geometric mean of a_{ij} and a_{ji}. In particular, Schwenk found that

$$\rho(\mathbf{G}) \leq \rho(\mathbf{A}). \tag{15}$$

A simple proof of this inequality can be found in Alpin and Merikoski (2010).

For a symmetric matrix $\mathbf{G}$, the Rayleigh quotient

$$R(\mathbf{G}, \mathbf{u}) \equiv \frac{\mathbf{u}^T\mathbf{G}\mathbf{u}}{\mathbf{u}^T\mathbf{u}} \tag{16}$$

is equal to $\rho(\mathbf{G})$ when $\mathbf{u}$ is the eigenvector associated with the dominant eigenvalue of $\mathbf{G}$; for all other $\mathbf{u}$, the Rayleigh quotient will be less than $\rho(\mathbf{G})$. Kolotilina (1993) used this property to propose a simple, easily calculable lower bound for $\rho(\mathbf{G})$, given by

$$\frac{\mathbf{e}^T\mathbf{G}\mathbf{e}}{m} \leq \rho(\mathbf{G}) \leq \rho(\mathbf{A}), \tag{17}$$

where $\mathbf{e} = (1, \ldots, 1)^T$, a vector of ones with length m.

Schwenk's and Kolotilina's results are relevant to us for two reasons. First, we can approximate an asymmetric dispersal kernel with a nonnegative, asymmetric matrix, a common approach for numerical analysis. Kot and Phillips (2015) detail one such method for discretizing $k(x, y)$ into an $m \times m$ matrix $\mathbf{K}$. Applying this discretization to Eq. 7 yields the eigenvalue problem

$$\lambda\mathbf{u} = R_0\mathbf{K}\mathbf{u}. \tag{18}$$

Second, the Rayleigh quotient approximation of $\rho(\mathbf{A})$ can likewise be used to approximate $\rho(R_0\mathbf{K})$, which is precisely the dominant eigenvalue we desire to describe persistence. Hence, these results provide us with a simple method for estimating the eigenvalue that determines persistence in a population with asymmetric dispersal.

Let us now formalize the notion of geometric symmetrization for a continuous kernel $k(x, y)$. We start by defining the *geometric success function* $G(y)$ as

$$G(y) \equiv \int_\Omega \sqrt{k(x, y)k(y, x)}\, dx. \tag{19}$$

When $k(x, y)$ is symmetric, $G(y) = s(y) = r(y)$, since $k(x, y) = k(y, x)$ implies that $\sqrt{k(x, y)k(y, x)} = k(x, y)$. As $k(x, y)$ becomes increasingly asymmetric, $s(y)$ and $r(y)$ diverge from one another, and $G(y)$ diverges from both (Fig. 1). Averaging $G(y)$ over Ω gives us the geometric symmetrization of the average dispersal success S, defined as

$$GS \equiv \frac{1}{|\Omega|}\int_\Omega G(y)\, dy = \frac{1}{|\Omega|}\int_\Omega\int_\Omega \sqrt{k(x, y)k(y, x)}\, dxdy. \tag{20}$$

Kot and Phillips (2015) observed that GS is the continuous form of the Rayleigh quotient in Eq. 17, i.e.,

$$GS = \lim_{m\to\infty} \frac{\mathbf{e}^T\mathbf{G}\mathbf{e}}{m} = \frac{\int_\Omega\int_\Omega \sqrt{k(x, y)k(y, x)}\, dx\, dy}{\int_\Omega 1\, dy} \tag{21}$$

$$= \frac{1}{|\Omega|}\int_\Omega\int_\Omega \sqrt{k(x, y)k(y, x)}\, dx\, dy, \tag{22}$$

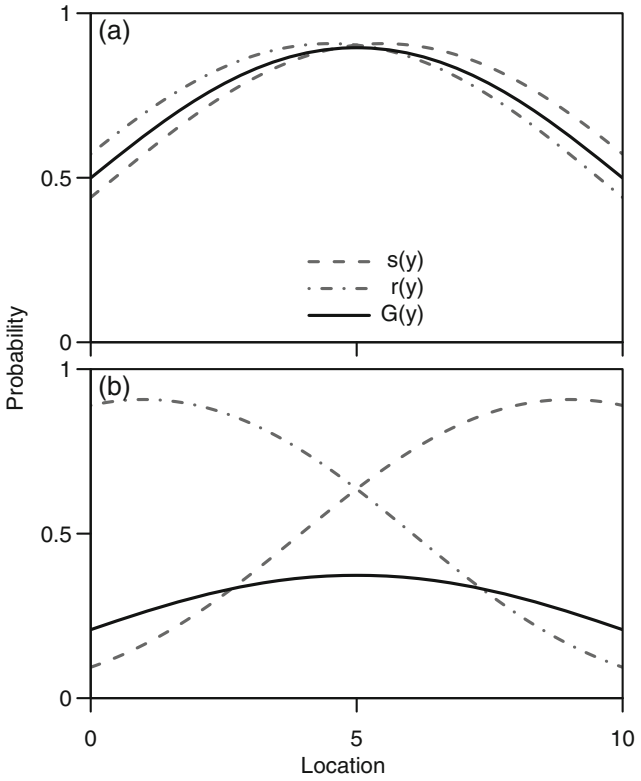

Fig. 1 Dispersal success function $s(y)$, redistribution function $r(y)$, and geometric success function $G(y)$ of a shifted Gaussian kernel with $\sigma = 3$ on the domain $\Omega = [0, 10]$ for varying c. In **a** $c = 0.5$, and $s(y)$ and $r(y)$ are relatively close in value in Ω. In **b** $c = 4$, and $s(y)$ and $r(y)$ diverge from one another. S is the spatial average of $s(y)$ (equivalently, $r(y)$) across Ω, whereas GS is the spatial average of $G(y)$

where m is again the number of discrete points in Ω and with the elements of $\mathbf{G}$ given by $g_{ij} = \sqrt{k_{ij}k_{ji}}$. This observation, along with Kolotilina's result in Eq. 17, guarantees that GS provides a lower-bound approximation of the dominant eigenvalue of Eq. 6.

How might we interpret the value of GS biologically? If we begin with an initial population N_0 uniformly distributed across Ω, then the spatial distribution of individuals after one time step is described by $r(y)$, and the average dispersal success S reflects the proportion $P_1 = N_1/N_0$ of population left in Ω after one time step. Similarly, the modified average dispersal success $\widehat{S}$ reflects the proportion of population left in Ω after one time step assuming an initial distribution of $r(y)$, or, equivalently, the ratio $P_2 = N_2/N_1$ of populations between the first and second time steps. Repeating the dispersal process over multiple time steps yields the sequence $P_3, P_4, P_5, \ldots$. As $t \to \infty$, eventual extirpation occurs if $P_t \to 0$. If the population converges to an equilibrium, then the sequence is bounded below by GS. Thus, we can interpret GS as an estimate of the proportion of individuals that remain in Ω after dispersal when the population has reached equilibrium. If the population dies out, then $GS = 0$; if $GS > 0$, then the population is able to persist.

To illustrate this, we simulated the process of repeated dispersal on a patch of length $L = 10$. We began with a population $N_0(x)$ of $N_0 = 1\,000\,000$ individuals distributed uniformly across $\Omega = [0, 10]$. Dispersal distances were randomly drawn from a shifted Gaussian kernel (see Table 1) with $\sigma = 2$, and added to $N_0(x)$ to simulate dispersal. P_1 was then calculated as the proportion of individuals left inside of Ω after the dispersal event. The locations of the individuals that dispersed successfully (i.e., stayed inside the patch) were then randomly resampled to replace the number of individuals lost due to dispersal, to give us our new population $N_1(x)$, such that the population stayed constant (i.e., $N_0 = N_1$). Resampling allowed us to iterate the process of dispersal indefinitely without running out of individuals, while capturing the desired sequence of population ratios $P_1, P_2, P_3, \ldots$ that reflect the population losses due to dispersal at each time step. We replicated this process for 61 different shift speeds ranging from $c = 0$ to $c = 6$. A comparison of the proportion of individuals remaining in the patch for the first eight time steps and the values of S, $\widehat{S}$, and GS can be seen in Fig. 2.

Returning to our mathematical discussion, we note that Kolotilina (1993) further proposed a sequence of lower bounds that improve the approximation of $\rho(\mathbf{A})$, given by

$$\frac{\mathbf{e}^T\mathbf{G}\mathbf{e}}{m} \le \left(\frac{\mathbf{e}^T\mathbf{G}_2\mathbf{e}}{m}\right)^{1/2} \le \cdots \le \left(\frac{\mathbf{e}^T\mathbf{G}_{2^k}\mathbf{e}}{m}\right)^{2^{-k}} \le \rho(\mathbf{A}), \tag{23}$$

where $\mathbf{G}_n$ is the geometric symmetrization of $\mathbf{A}^n$, such that $(g_n)_{ij} = \sqrt{a^n_{ij}a^n_{ji}}$, with a^n_{ij} the ij-th element of $\mathbf{A}^n$. It can likewise be seen that

$$\lim_{m\to\infty}\left(\frac{\mathbf{e}^T\mathbf{G}_n\mathbf{e}}{m}\right)^{n^{-1}} = \left(\frac{\int_\Omega\int_\Omega \sqrt{k^n(x,y)k^n(y,x)}\,dx\,dy}{\int_\Omega 1\,dy}\right)^{n^{-1}} \tag{24}$$

$$= \left(\frac{1}{|\Omega|}\int_\Omega\int_\Omega \sqrt{k^n(x,y)k^n(y,x)}\,dx\,dy\right)^{n^{-1}}, \tag{25}$$

where $k^n(x, y)$ is the *nth iterated kernel* of $k(x, y)$ (Zabreyko et al. 2013), defined recursively such that

$$k^1(x, y) = k(x, y), \tag{26}$$

$$k^n(x, y) = \int_\Omega k(x, z)k^{n-1}(z, y)\,dz. \tag{27}$$

Table 1 Discrete-time growth functions and dispersal kernels considered in this paper (Adapted from Reimer et al. 2016)

Growth functions		
Beverton-Holt	$N_{t+1} = \frac{R_0 N_t}{1+\frac{R_0-1}{K}N_t}$	Compensatory (Beverton and Holt 1957)
Logistic	$N_{t+1} = N_t + rN_t\left(1-\frac{N_t}{K}\right)$	Overcompensatory (May and Oster 1976)
Ricker	$N_{t+1} = N_t \exp\left[r\left(1-\frac{N_t}{K}\right)\right]$	Overcompensatory (Ricker 1954)
Dispersal kernels		
Shifted Gaussian	$k(x,y) = \frac{1}{\sqrt{2\pi\sigma^2}}\exp\left(-\frac{(x+c-y)^2}{2\sigma^2}\right)$	(Lutscher et al. 2005; Kot and Phillips 2015)
Shifted Laplace	$k(x,y) = \frac{1}{2b}\exp\left(-\frac{\lvert x+c-y\rvert}{b}\right)$	(Lutscher et al. 2005; Kot and Phillips 2015)
Shifted Cauchy	$k(x,y) = \left[\pi\gamma\left(1+\left(\frac{x+c-y}{\gamma}\right)^2\right)\right]^{-1}$	(Lutscher et al. 2005)
Asymmetric Laplace	$k(x,y) = \begin{cases} A\exp(a_1(x-y)), & x \le y \\ A\exp(a_2(x-y)), & x > y \end{cases}$	(Lutscher et al. 2005)

The iterated kernel $k^n(x,y)$ is analogous to the iterated dispersal matrix $\mathbf{K}^n$. The second iterated kernel $k^2(x,y)$ of the shifted Laplace kernel, for example, is

$$k^2(x,y) = \frac{1}{4b^2}\int_0^L e^{-\frac{|x+c-z|}{b}} e^{-\frac{|z+c-y|}{b}}\,dz \tag{28}$$

$$= \frac{1}{8b}\left(2e^{-s} + 2se^{-s} - e^{-\left(\frac{x+y}{b}\right)} - e^{-\left(\frac{2L-x-y}{b}\right)}\right), \tag{29}$$

with $s = \left|\frac{x+2c-y}{b}\right|$.

We may now generalize the formula for GS in Eq. 20 to

$$G_nS \equiv \left(\frac{1}{|\Omega|}\int_\Omega\int_\Omega \sqrt{k^{2^n}(x,y)k^{2^n}(y,x)}\,dx\,dy\right)^{2^{-n}}, \tag{30}$$

which provides increasingly tight lower bounds of the dominant eigenvalue of Eq. 6 for increasing n. We note that GS defined in Eq. 20 is equivalent to G_0S in Eq. 30; for the remainder of this paper, we will use the notation GS to refer to G_0S, and G_nS to refer to any value of n other than $n = 0$. For many parameter values, G_0S provides a perfectly adequate approximation of dispersal success.

In the next section, we will demonstrate that GS is a far more useful tool for describing the effects of asymmetric dispersal than either Van Kirk and Lewis' average dispersal success S or Reimer's modified $\widehat{S}$ (see Table 2 for reference).

Applications to integrodifference models

Consider the integrodifference equation

$$N_{t+1}(x) = \int_\Omega k(x,y)f[N_t(y)]\,dy, \tag{31}$$

and assume that $k(x,y)$ is asymmetric. With geometric symmetrization in hand, we are now equipped with a blueprint for constructing a symmetric kernel $\sqrt{k(x,y)k(y,x)}$ from $k(x,y)$. Furthermore, under certain assumptions on f and $k(x,y)$ (Zhou and Kot 2011), we know that the persistence criteria of

$$N_{t+1}(x) = \int_\Omega \sqrt{k(x,y)k(y,x)}\,f[N_t(y)]\,dy. \tag{32}$$

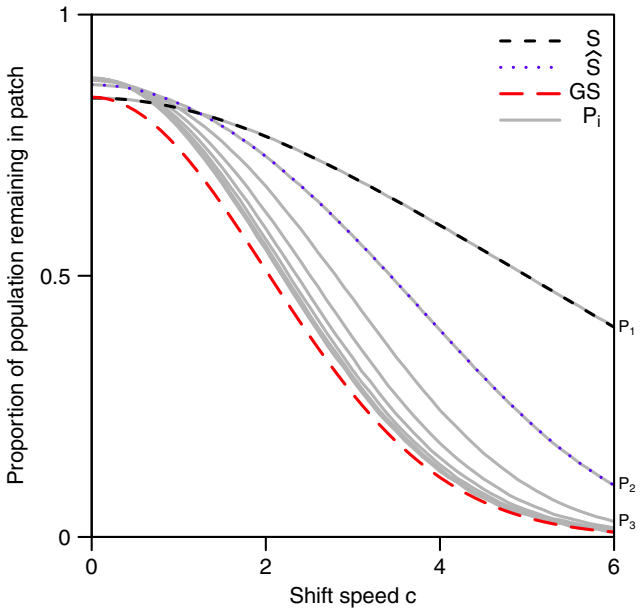

Fig. 2 The proportions of eight generations of individuals remaining in a patch of length 10, assuming shifted Gaussian dispersal with $\sigma = 2$, averaged over 100 simulations for each value of c. Each simulation began with initial population $N_0 = 1\,000\,000$ distributed randomly and uniformly across Ω. After dispersal, each generation was bootstrapped back to the initial population size, providing a sufficient growth rate to repeat the process of dispersal indefinitely. The proportion remaining after the first time step $P_1 = N_1/N_0$ is indistinguishable from the average dispersal success S. The ratio of populations between the first and second time step $P_2 = N_2/N_1$ is indistinguishable from the modified average dispersal success $\widehat{S}$. The sequence of population ratios between each successive time step P_3, P_4, P_5, ... approaches the geometric symmetrization GS of S

Table 2 Dispersal success approximations considered in this paper

Average dispersal success	S	(12)	Proportion of individuals staying in patch after single dispersal event (Van Kirk and Lewis 1997)
Modified S	$\widehat{S}$	(13)	Weights S by population density (Reimer et al. 2016)
Geometric symmetrization of S	$G_n S$	(30)	Proportion of individuals staying in patch after dispersal event at equilibrium (Kot and Phillips 2015)

will be close in value to the persistence criteria of Eq. 31. Although these two equations utilize different kernels, their dominant eigenvalues are approximately equal, which determines the criteria for population persistence. Finally, we have a simple method for approximating $\lambda_{\max}$ for Eq. 31, given by

$$\lambda_{\max} \approx \lambda_{GS} \equiv \frac{R_0}{|\Omega|}\int_\Omega\int_\Omega \sqrt{k(x,y)k(y,x)}\,dx\,dy \tag{33}$$

$$= R_0 GS, \tag{34}$$

which we can use to better understand how different model parameters relate to persistence. To illustrate, we turn again to shifted kernels of the form $k(x, y) = k(x + c - y)$.

Approximating the critical speed c^*

The critical speed c^* beyond which the population can no longer persist corresponds to the bifurcation value of $\lambda_{\max} = 1$; when $c > c^*$, $\lambda_{\max} < 1$, the population will die out.

For some dispersal kernels, the formulae for the various dispersal success approximations are simple enough to solve analytically. The shifted Laplace kernel (Table 1), for example, can be plugged into Eq. 12 to get

$$S = \begin{cases} 1 - \frac{c}{L} - \frac{be^{-c/b}}{L} + \frac{be^{-L/b}}{L}\cosh\left(\frac{c}{b}\right), & c < L, \\ \frac{be^{-c/b}}{L}\left(\cosh\left(\frac{L}{b}\right) - 1\right), & c \geq L. \end{cases} \tag{35}$$

Likewise, Eq. 20 gives

$$GS = \begin{cases} \frac{1}{L}\left[be^{-L/b} + e^{-c/b}\left(L - c - b + \frac{cL}{b} - \frac{c^2}{2b}\right)\right], & c < L, \\ \frac{1}{2b}e^{-c/b}L, & c \geq L. \end{cases} \tag{36}$$

Using the approximation of $\lambda_{\max} \approx \lambda_S = R_0 S$ in Eq. 9, we can substitute (35) into (9) and set $\lambda_S = 1$ to get

$$1 = R_0\left[1 - \frac{c^*}{L} - \frac{be^{-c^*/b}}{L} + \frac{be^{-L/b}}{L}\cosh\left(\frac{c^*}{b}\right)\right]. \tag{37}$$

From this, we can derive an expression for R_0 in terms of c^* and the model parameters L and b,

$$R_0 = \frac{L}{L - c^* - be^{-c^*/b} + e^{-L/b}\cosh\frac{c^*}{b}}, \tag{38}$$

assuming that $c^* < L$. Similarly, the formula for λ_{GS} in Eq. 34 for GS implies

$$R_0 = \frac{L}{be^{-L/b} + e^{-c^*/b}\left(L - c^* - b + \frac{c^*L}{b} - \frac{c^{*2}}{2b}\right)}. \tag{39}$$

Applying L'Hôpital's rule to Eq. 39 as $L \to \infty$, this equation predicts limiting curves of

$$R_0 = \frac{e^{c^*/b}}{1 + \frac{c^*}{b}}. \tag{40}$$

For a given growth rate R_0, this curve approximates the invasion speed p^* of an IDE with an infinite domain, described parametrically in Kot et al. (2004) as

$$p^* = \frac{2ub^2}{1 - u^2b^2}, \tag{41}$$

$$R_0 = \left(1 - u^2b^2\right)\exp\left(\frac{2u^2b^2}{1 - u^2b^2}\right), \tag{42}$$

as can be seen in Fig. 3.

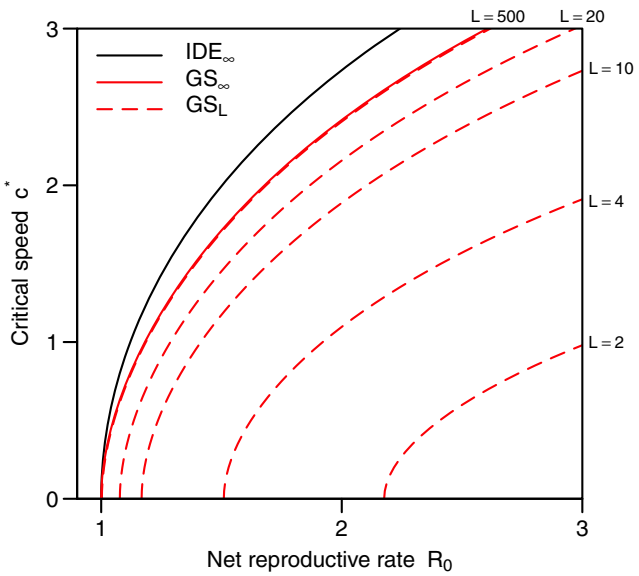

Fig. 3 Critical speed curves GS_L for a shifted Laplace kernel with $b = 1.44$ predicted using GS (dashed red lines) for a variety of domain sizes, compared with the invasion speed IDE_∞ on an infinite domain predicted by Eqs. 41 and 42 (solid gray line) and the approximation GS_∞ of the invasion speed on an infinite domain provided by Eq. 40 (solid red line)

For kernels less amenable to analytic evaluation, it remains quite straightforward to use numerical optimization to solve $1 = R_0 S$, and likewise, the corresponding equations for $\widehat{S}$ and GS. To illustrate, we numerically calculated c^* for IDEs discretized at $m = 101$ points on a patch of length 10, using R's `optimize` function (R Core Team 2017) to minimize the quantity

$$|\rho(R_0\mathbf{K}) - 1| \tag{43}$$

for different values of R_0, and compared this critical speed curve with the critical speed curves derived by minimizing

$$|R_0 S - 1|, \tag{44}$$
$$|R_0 \widehat{S} - 1|, \tag{45}$$
$$|R_0 G_n S - 1|, \tag{46}$$

for S, $\widehat{S}$, and $G_n S$, respectively, for various R_0, with increasingly accurate estimates of $\lambda_{\max}$ provided by $G_n S$ for increasing n. Figure 4 compares the results for three different shifted kernels, using dispersal parameters $\sigma = 1.48$ (Gaussian), $\gamma = 1$ (Cauchy), $b = 1.44$ (Laplace) so that each kernel has the same median absolute deviation when $c = 0$ (Rousseeuw and Croux 1993). Figure 4 shows that $G_0 S$ more closely approximates the critical speed curve of a numerically approximated IDE of the form found in Eq. 6 for the chosen parameter values than S or $\widehat{S}$, and this approximation can be considerably improved with $G_1 S$. These patterns are consistently observable across a wide range of parameter values.

All other parameters being equal, $G_n S$ also correctly predict higher critical speeds for kernels with higher kurtosis κ, a measure of the "fatness" of tails. (We note that although the Cauchy distribution does not have finite kurtosis on an unbounded domain, its kurtosis is finite on the bounded domain $\Omega = [0, L]$.) In contrast, kurtosis does not appear to have a significant effect on estimates of c^* derived with S or $\widehat{S}$. Table 3 compares estimates of c^* for an IDE with $L = 100$, $R_0 = 1.8$, and $\sigma = 2 \cdot 1.48$ (Gaussian), $\gamma = 2$ (Cauchy), and $b = 2 \cdot 1.44$ (Laplace). These estimates illustrate how long-distance dispersal can influence persistence: the Gaussian kernel ($\kappa = 3$ for $c = 0$) has the thinnest tails of the three, signifying a low probability of long-distance dispersal events, and hence has the smallest critical speed. The Cauchy kernel ($\kappa \approx 15$ for $c = 0$) has the fattest tails of the three, meaning that long-distance dispersal events are much more likely, making it possible for the population to persist at much higher shift speeds. The Laplace distribution ($\kappa = 6$ for $c = 0$) falls somewhere in between.

Approximating the critical domain size L^*

Just as Eqs. 35 and 36 enabled us to explore the relationship between the intrinsic growth rate R_0 and the critical speed

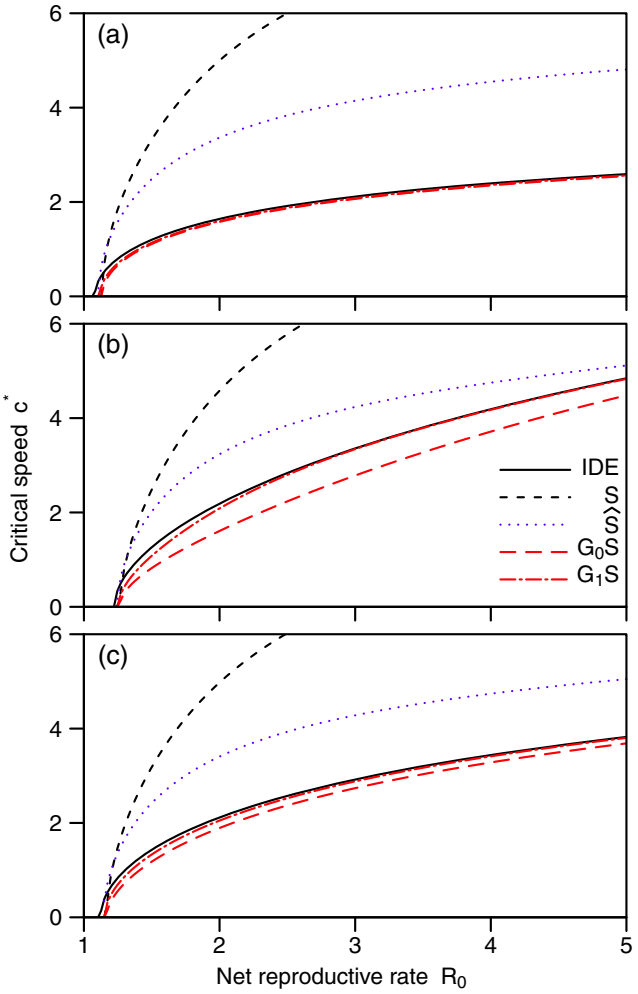

Fig. 4 Numerical approximations of critical speed curves for **a** a shifted Gaussian kernel with $\sigma = 1.48$, **b** a shifted Cauchy kernel with $\gamma = 1$, and **c** a shifted Laplace kernel with $b = 1.44$, and with $L = 10$

c^*, so may they help us determine the critical domain size L^*. We use Eqs. 38 and 39 to plot L^* as a function of c for various values of R_0 (Fig. 5).

Again, the same numerical techniques used for solving $1 = R_0 S$ (and the corresponding equations for $\widehat{S}$ and $G_n S$) for c^* apply just as readily to solving $1 = R_0 S$ for L^*. Minimizing (43) for different values of c yields a critical

Table 3 Different estimates of the critical speed c^* of an IDE with $L = 100$, $R_0 = 1.8$, $\sigma = 2 \cdot 1.48$ (Gaussian), $\gamma = 2$ (Cauchy), and $b = 2 \cdot 1.44$ (Laplace). c^* increases with the kurtosis of the kernel

	Numeric	S	$\widehat{S}$	$G_0 S$	$G_1 S$	$G_2 S$
Gaussian	3.2	40.0	30.8	3.1	3.2	3.2
Laplace	4.9	40.0	30.8	4.1	4.5	4.7
Cauchy	12.6	40.0	30.4	4.3	8.1	12.2

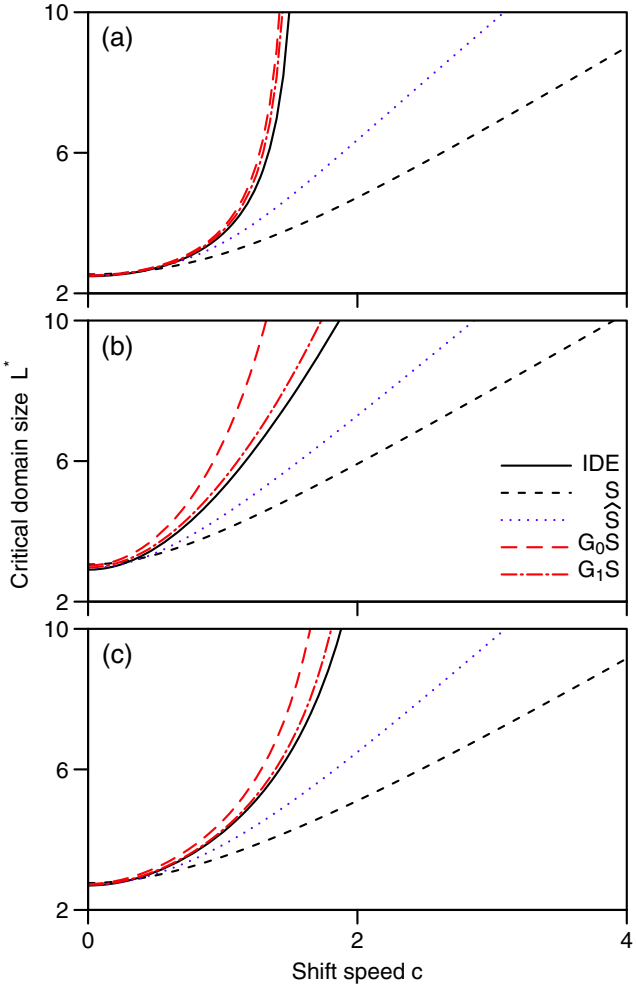

Fig. 5 Numerical approximations of critical domain size for a shifted Gaussian kernel with $\sigma = 1.48$, a shifted Cauchy kernel with $\gamma = 1$, and a shifted Laplace kernel with $b = 1.44$, and with $R_0 = 1.8$

domain size curve, and minimizing (44), (45), (46) similarly yield critical domain size curves as a function of S, $\widehat{S}$, and G_nS, respectively. Figure 5 compares these critical domain size curves for three different shifted kernels, again using dispersal parameters $\sigma = 1.48$ (Gaussian), $\gamma = 1$ (Cauchy), $b = 1.44$ (Laplace), and with $R_0 = 1.8$. As with critical speed in Fig. 4, Fig. 5 illustrates that G_1S most closely approximates the critical domain size curve of the numerically approximated IDE for the chosen parameter values, and this can be observed for other parameter values as well.

Approximating mean population density at equilibrium

Let us assume that (31) has a nontrivial equilibrium solution $N^*(x)$ such that

$$N^*(x) = \int_\Omega k(x, y) f[N^*(y)]\, dy. \tag{47}$$

By applying ADS to Eq. 47, we can approximate the effects of $k(x, y)$ with S by averaging the cumulative effects of dispersal over the domain. This method reduces the equilibrium solution of the IDE to its spatial average, which can then be used to describe persistence more explicitly. This technique is detailed in Lutscher and Lewis (2004), but we outline the process here.

We begin by averaging the population distribution $N_t(x)$ over the spatial domain, which we denote as

$$\overline{N}_t \equiv \frac{1}{|\Omega|}\int_\Omega N_t(x)\, dx. \tag{48}$$

Applying this average to both sides of Eq. 31 yields

$$\frac{1}{|\Omega|}\int_\Omega N_{t+1}(x)\, dx = \frac{1}{|\Omega|}\int_\Omega\int_\Omega k(x, y) f[N_t(y)]\, dx\, dy. \tag{49}$$

The first-order Taylor expansion of f about $\overline{N}_t$ is

$$f[N_t(x)] \approx f[\overline{N}_t] + f'[\overline{N}_t]\left(N_t(x) - \overline{N}_t\right). \tag{50}$$

If the difference between the nonzero equilibrium $N^*(x)$ and the spatial average $\overline{N}_t$ of $N_t(x)$ is small, i.e., if the spatial average $\overline{N}_t$ is close to equilibrium, then we may neglect the linear term in Eq. 50 and approximate f by

$$f[N_t(x)] \approx f[\overline{N}_t]. \tag{51}$$

Substituting (51) into (49) yields

$$\frac{1}{|\Omega|}\int_\Omega N_{t+1}(x)\, dx \approx f[\overline{N}_t]\frac{1}{|\Omega|}\int_\Omega\int_\Omega k(x, y)\, dx\, dy, \tag{52}$$

which implies that $\overline{N}_t$ changes over time as

$$\overline{N}_{t+1} \approx S \cdot f[\overline{N}_t]. \tag{53}$$

In this manner, we may approximate an IDE by averaging over space, which separates the dispersal kernel and growth function into individual, more digestible components. In the case of a Beverton-Holt growth curve (Table 1), the spatial average of the nontrivial equilibrium solution of Eq. 31 is approximated by

$$\overline{N}^*_S = \frac{K(SR_0 - 1)}{R_0 - 1}. \tag{54}$$

Note the similarities between this and the fixed point of the nonspatial Beverton-Holt model, $N^* = \frac{K(R_0-1)}{R_0-1} = K$. Similarly, the spatial averages of the logistic and Ricker growth functions are approximated by

$$\overline{N}^*_S = \frac{SK(1 + r) - K}{Sr}, \tag{55}$$

and

$$\overline{N}^*_S = K\left(\frac{\log S}{r} + 1\right), \tag{56}$$

respectively.

As we've already seen in other examples, approximations derived using S do not extend well to the case of asymmetric dispersal. Indeed, it is quite easy to verify that (54), (55), and (56) can substantially overestimate the mean equilibrium $\overline{N^*(x)}$ of an IDE with asymmetric dispersal. We may, however, derive similar estimates of $\overline{N^*(x)}$ in terms of GS by applying similar reasoning to the integrodifference model

$$N_{t+1}(x) = \int_\Omega \sqrt{k(x,y)k(y,x)}\, f[N_t(y)]\, dy. \tag{57}$$

Following the same process as before, $\overline{N}$ now changes over time as

$$\overline{N}_{t+1} \approx GS \cdot f[\overline{N}_t]. \tag{58}$$

This yields the estimates

$$\overline{N^*_{GS}} = \frac{K(GSR_0 - 1)}{R_0 - 1}, \tag{59}$$

$$\overline{N^*_{GS}} = \frac{GSK(1+r) - K}{GSr}, \tag{60}$$

$$\overline{N^*_{GS}} = K\left(\frac{\log GS}{r} + 1\right), \tag{61}$$

for the the spatial averages of the Beverton-Holt, logistic, and Ricker growth functions, respectively. Similar estimates may also be found approximating the equilibrium $\overline{N^*_{\widehat{S}}}$ in terms of $\widehat{S}$.

Why might we expect (57) to have similar average population densities as Eq. 31 at equilibrium? To answer this question, we consider the kernel $k(x, y)$, and note that

$$k(x,y) = \sqrt{k(x,y)k(x,y)} \tag{62}$$

$$= \sqrt{k(x,y)k(y,x) + k(x,y)\,(k(x,y) - k(y,x))}. \tag{63}$$

Assuming the quantity $k(x, y)\,(k(x, y) - k(y, x))$ is small, then applying the linear approximation

$$\sqrt{x+\epsilon} \approx \sqrt{x} + \frac{1}{2\sqrt{x}}\epsilon \tag{64}$$

to Eq. 63 yields

$$k(x,y) \approx \sqrt{k(x,y)k(y,x)} + \frac{1}{2}\sqrt{\frac{k(x,y)}{k(y,x)}}\,(k(x,y) - k(y,x)) \tag{65}$$

$$\approx \sqrt{k(x,y)k(y,x)}. \tag{66}$$

Thus, Eq. 57 can be seen as a lower order approximation of Eq. 31. For shifted kernels, the quantity $k(x, y) - k(y, x)$ should be small for smaller values of c, since $k(x, y) \approx k(y, x)$ when $k(x, y)$ is close to symmetric. For larger values of c, we already know that Eq. 57 has approximately identical persistence criteria as Eq. 31, so we should expect the two to have similar population densities as c approaches the critical speed c^*, and equal densities for $c \geq c^*$. In this

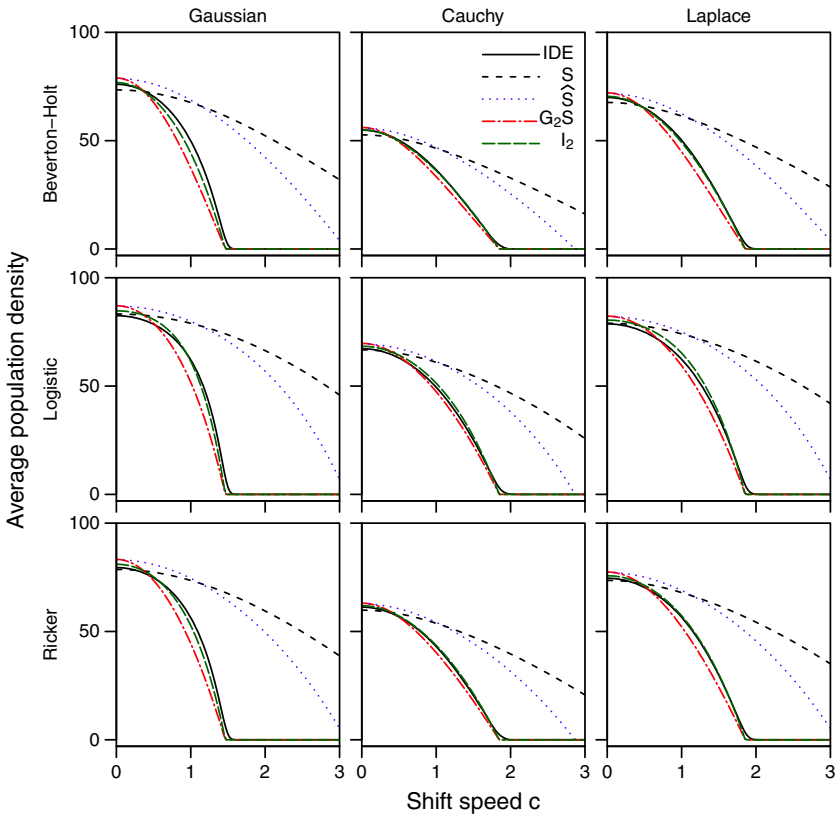

Fig. 6 A comparison of the spatial averages of the nontrivial equilibrium solutions of an IDE with a variety of growth functions and a variety of shifted dispersal kernels, with $L = 10$, $K = 100$, $R_0 = 1.8$ (Beverton-Holt), $r = 0.8$ (logistic) and $r = \log(1.8)$ (Ricker), and $\sigma = 1.48$ (Gaussian), $\gamma = 1$ (Cauchy), and $b = 1.44$ (Laplace)

regard, we may reasonably expect that Eqs. 59, 60, and 61 provide more accurate estimates of mean population density for increasing c than Eqs. 54, 55, and 56.

In fact, we may further improve these estimates by calculating one more iteration of the integrodifference equation in Eq. 31. Taking $\overline{N^*_{GS}}$ as our estimate of $N^*(x)$, we get

$$N^*(x) = \int_\Omega k(x,y) f[N^*(x)]\,dy \tag{67}$$

$$\approx \int_\Omega k(x,y) f[\overline{N^*_{GS}}]\,dy \tag{68}$$

$$= \int_\Omega k(x,y) \frac{\overline{N^*_{GS}}}{GS}\,dy \tag{69}$$

$$= \frac{\overline{N^*_{GS}}}{GS} \int_\Omega k(x,y)\,dy. \tag{70}$$

Recognizing the integral in Eq. 70 as the redistribution function $r(x)$ from Eq. 11, we infer

$$N^*(x) \approx \frac{\overline{N^*_{GS}}}{GS} r(x). \tag{71}$$

This equation is similar in form to the *redistribution approximation* described by Lutscher and Lewis (2004), defined in terms of S as

$$N^*(x) \approx \frac{\overline{N^*}}{S} r(x). \tag{72}$$

Finally, averaging (71) across the domain yields the estimate

$$\overline{N^*(x)} \approx \frac{\overline{N^*_{GS}}}{GS} \int_\Omega r(x)\,dx \tag{73}$$

$$= \frac{S}{GS} \overline{N^*_{GS}}. \tag{74}$$

We denote the approximation in Eq. 74 as $\overline{N^*_I}$, or more generally for $G_n S$ as

$$\overline{N^*_{I_n}} = \frac{S}{G_n S} \overline{N^*_{G_n S}}. \tag{75}$$

Figure 6 shows estimates of the spatial average of the nonrivial equilibrium solution $\overline{N^*_S}$, $\overline{N^*_{\widehat{S}}}$, $\overline{N^*_{G_2 S}}$, and $\overline{N^*_{I_2}}$ for a variety of growth functions, dispersal kernels, and shift speeds. We quantified the accuracy of these estimates for two different domain sizes using the root-mean-square error (RMSE) between each estimate and the spatial average of the numerically calculated IDE equilibrium solution, calculated for equally spaced values of c ranging from $c = 0$ to $c = c^*_{all}$, the smallest value of c for which all four estimates predicted extinction. $\overline{N^*_{I_2}}$ provided the lowest RMSE in all but one scenario (Table 4), suggesting that it is the most accurate approximation of the four.

Figure 7 illustrates a more extreme example of Fig. 6, considering a shifted Cauchy distribution with $L = 100$, $R_0 = 1.8$, and $\gamma = 2$. In this case, patch size is considerably larger than the mean dispersal distance, but the fatter tails of the Cauchy distribution makes long-distance dispersal events more likely, and the critical speed c^* for persistence is considerably higher than for kernels with thinner tails (see Table 3). Figure 7 shows how estimates of the mean population at equilibrium based on $G_n S$ and I_n improve for increasing n. Although $G_n S$ and I_n significantly underestimate $\overline{N^*(x)}$ for $n = 0$, these estimates are considerably improved for $n = 1$, and quite respectable for $n = 2$. By $n = 3$, $\overline{N^*_{I_3}}$ is almost indistinguishable from $\overline{N^*(x)}$.

Table 4 Root-mean-square error between the spatial average of the numerically calculated IDE equilibrium solution and various approximations of the spatial average

Scenario				Root-mean-square error			
L	Dispersal	Growth	m	$\overline{N^*_S}$	$\overline{N^*_{\widehat{S}}}$	$\overline{N^*_{G_2 S}}$	$\overline{N^*_{I_2}}$
10	Gaussian	BH	89	32.5	24.6	4.7	**2.2**
		Logistic		41.6	31.3	4.5	**1.8**
		Ricker		37.0	28.0	4.6	**1.9**
	Cauchy	BH	79	18.4	13.1	1.5	**0.3**
		Logistic		26.1	18.4	1.4	**1.1**
		Ricker		22.1	15.6	1.5	**0.5**
	Laplace	BH	89	25.9	18.2	2.6	**0.5**
		Logistic		34.5	24.1	2.4	**1.5**
		Ricker		30.1	21.1	2.5	**0.6**
100	Gaussian	BH	90	54.0	48.4	9.3	**8.1**
		Logistic		62.6	55.3	8.3	**6.8**
		Ricker		58.4	51.9	8.8	**7.5**
	Cauchy	BH	89	40.6	33.7	11.1	**7.4**
		Logistic		49.7	40.9	9.2	**4.6**
		Ricker		45.1	37.3	10.3	**6.0**
	Laplace	BH	90	52.6	46.8	8.9	**7.2**
		Logistic		61.3	53.8	7.6	**5.4**
		Ricker		57.0	50.3	8.3	**6.3**

Each approximation was calculated for m equally spaced values from $c = 0$ to $c = c^*_{all}$, the smallest value of c for which all four estimates predicted extinction. Lowest values are in bold

Other types of asymmetry

So far, we have explored asymmetric dispersal primarily in the context of climate change, examining Zhou and Kot (2011)'s integrodifference model with shifted kernels, but there are several other possible mechanisms through which asymmetric dispersal can arise. Advection can act upon individuals in the form of wind, ocean, or stream currents (Lutscher et al. 2005), or the diffusion process itself may be biased in a particular direction due to physiological or morphological constraints (Levin et al. 2003). We will now

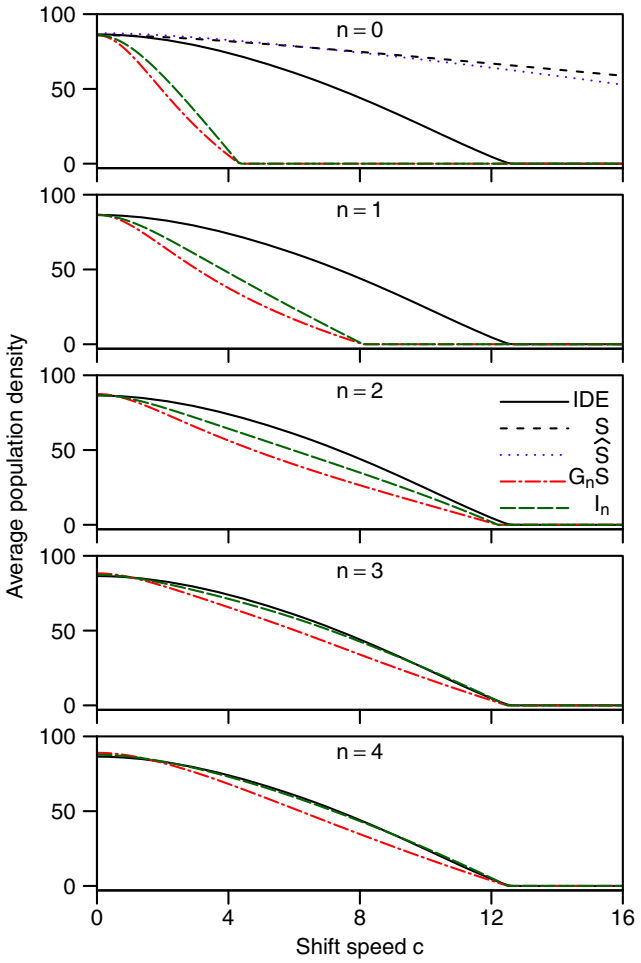

Fig. 7 A comparison of estimates of the spatial averages of population at equilibrium derived from $G_n S$ and I_n for increasing values of n, assuming Beverton-Holt dynamics with $R_0 = 1.8$, a shifted Cauchy kernel with $\gamma = 2$, and $L = 100$. As n increases, $G_n S$ and I_n provide increasingly accurate estimates of $\overline{N^*(x)}$. The top panel includes estimates based on S and $\widehat{S}$ for comparison, but these estimates do not change with n

demonstrate how the various metrics of dispersal success can be applied to a dispersal kernel subject to advection.

Lutscher et al. (2005) used a partial differential equation modeling the individual movement of aquatic insects in a stream habitat to derive a modified Laplace kernel that accounts for advection. This asymmetric Laplace kernel is given by

$$k(x, y) = \begin{cases} A \exp(a_1(x - y)), & x \le y, \\ A \exp(a_2(x - y)), & x > y, \end{cases} \tag{76}$$

where $a_{1,2} = v/2D \pm \sqrt{v^2/4D^2 + \alpha/D}$, with D the diffusion constant, $v \ge 0$ the advection velocity, and α a constant settling rate, and where $A = a_1 a_2/(a_2 - a_1) = \alpha/\sqrt{v^2 + 4\alpha D}$, which ensures that $k(x, y)$ integrates to 1. The advection velocity v is analagous to the shift speed c in the shifted Laplace, and the quantity $\sqrt{\frac{D}{\alpha}}$ is analagous to the shape parameter b. In a similar fashion, the shifted Gaussian and shifted Cauchy can be seen as specific cases of the more general formulae

$$k(x, y) = \frac{1}{\sqrt{4\pi\alpha D}} \exp\left(-\frac{(x + \alpha v - y)^2}{4\alpha D}\right) \tag{77}$$

and

$$k(x, y) = \left[\frac{\pi\gamma}{\alpha}\left(\alpha^2 + \left(\frac{x + \alpha v - y}{\gamma}\right)^2\right)\right]^{-1}, \tag{78}$$

respectively, with $2\alpha D = \sigma^2$ and $\alpha = 1$ (Reimer et al. 2016).

The average dispersal success of the asymmetric Laplace is

$$S = \frac{A(e^{-a_1 L} + a_1 L - 1)}{L a_1{}^2} - \frac{A(a_2 L - e^{a_2 L} + 1)}{L a_2{}^2}, \tag{79}$$

and the geometric symmetrization of S is

$$GS = \frac{2A}{B} + \frac{2A}{B^2 L}\left(e^{-BL} - 1\right), \tag{80}$$

where $B = \frac{a_1 - a_2}{2}$. We note that Reimer et al. (2016) provides a formula for $\widehat{S}$ for the asymmetric Laplace, which we will not reproduce here.

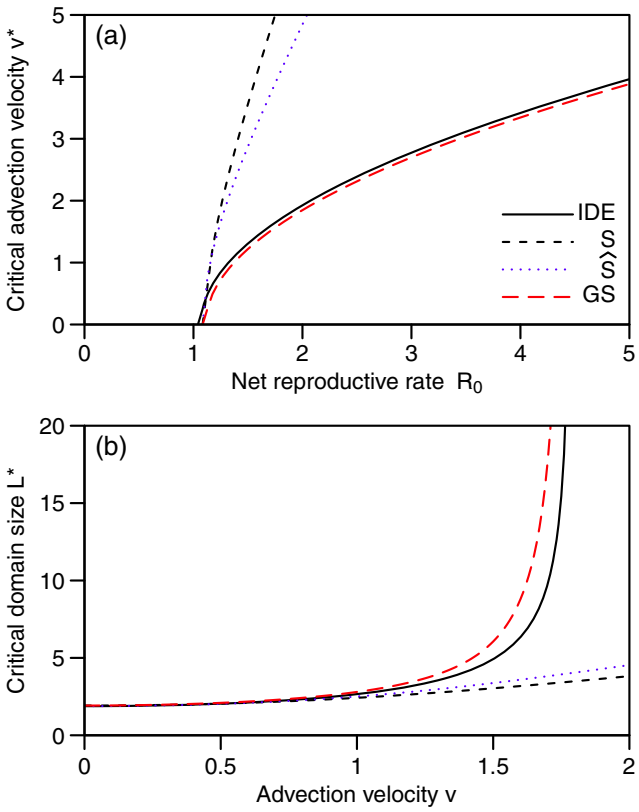

Fig. 8 Approximations of **a** the critical advection velocity v^* of an IDE with $\alpha = 1$, $D = 1$, and $L = 10$, and **b** the critical domain size L^* of an IDE with $R_0 = 1.8$ and an asymmetric Laplace dispersal kernel with $\alpha = 1$, $D = 1$

We may once again use these formulae to calculate the critical domain size L^* or the critical advection velocity v^*. Substituting (79) into $\lambda_S = R_0 S$ and setting $\lambda_S = 1$ yields

$$R_0 = \frac{La_1{}^2a_2{}^2}{A(e^{-a_1 L} + a_1 L - 1) - A(a_2 L - e^{a_2 L} + 1)}. \quad (81)$$

Similarly, substituting (80) into $\lambda_{GS} = R_0 GS$ and setting $\lambda_{GS} = 1$ yields

$$R_0 = \frac{B^2 L}{2A\left(BL + e^{-BL} - 1\right)}. \quad (82)$$

Comparisons of estimates of L^* and v^* can be seen in Fig. 8.

Discussion

Dispersal is a complicated process. Dispersal takes place at the scale of the individual, and is inevitably influenced by a multitude of factors that affect the individual, such as habitat heterogeneity in both space and time, and demographic and environmental stochasticity. Modeling dispersal at the scale of the individual necessitates tracking each individual through time and space, but this method is often constrained by computational power, and this limitation grows with model complexity (Snyder 2003). In many situations, it behooves us to focus our efforts on modeling emergent population properties that result from the aggregate effects of individual dispersal. At the expense of granularity, modeling cumulative population behavior greatly simplifies the task of understanding how process affects pattern (Rahmandad and Sterman 2008). Average dispersal success is one such example of an emergent property, describing the aggregate effects of dispersal within a population over the course of a generation, and, asymptotically, population persistence.

In addition to the distinction between modeling the individual vs. modeling the population is the contrast in using numerical analysis or analytic methods to obtain results. One of the benefits of the analytic approach is that an analytic solution can oftentimes more succinctly illuminate the relationships between a model's components. In the fortuitous (and admittedly rare) circumstance of possessing an analytic solution to an IDE model, one can see precisely how a population scales with the tweaking of a parameter or the value of a variable. Of course, many (if not most) integrodifference equations do not lend themselves kindly to analytic approaches, and numerical methods are more common (Zhou and Kot 2011). Prudent and judicious applications of analytic approximations, however, provide us another way forward. By averaging the spatial aspects of integrodifference equations, we found a family of approximations of the dominant eigenvalue that determines population persistence. This sacrifice of spatial explicitness is of little consequence if we are not concerned with *where* individuals are in space, but simply that they *are*.

The benefits of such approximations are further evident in the simplicity of equations such as

$$\lambda_{\max} \approx R_0 G_n S \quad (83)$$

in Eq. 34. The integrodifference equation of Zhou and Kot (2011) in Eq. 6 is a convolution of the growth and dispersal processes, and (to paraphrase one of the authors) generates a nasty eigenvalue problem (Kot and Phillips 2015). In contrast to this nastiness, Eq. 83 elegantly decouples the growth and dispersal components, and in doing so, illuminates how dispersal success and growth rate each relate to population persistence. Moreover, this approximation appears to be quite accurate.

We highlighted the fact that dispersal is, more often than not, an asymmetric process. With asymmetric dispersal, the aggregate effects of individual dispersal events appear as a bias for the population to move in a certain direction, be it in latitude, elevation, slope, along ocean currents, or stream flow. Any such metric that hopes to meaningfully quantify a population's dispersal through space and time must account for this asymmetry. We asserted that the original definition of average dispersal success in Van Kirk and Lewis (1997) does not adequately reflect the effects of asymmetric dispersal, but we explored how to address this shortcoming using geometric symmetrization.

One of the benefits of average dispersal success S is that it can be estimated experimentally through obervation of population dispersal without explicit knowledge of $k(x, y)$. This is due to its simple ecological interpretation as the proportion of individuals remaining after a single dispersal event. We provided a similar interpretation of GS as the proportion of individuals remaining after dispersal when the population is at equilibrium. This suggests that GS can also be estimated experimentally without knowledge of $k(x, y)$ through repeated observation of population dispersal events over time, thus providing a practical method for inferring persistence criteria from empirical data.

It is also worth acknowledging the importance of long-distance dispersal events in determining the rates and extents of spread of populations. Dispersal events are frequently observed at distances and frequencies greater than those predicted by a normal distribution, and kernels fit to observation data are typically characterized by fatter tails (Nathan et al. 2003). Kot et al. (1996) demonstrated how long-distance dispersal can affect the rate of spread of a population of fruit flies; fat-tailed kernels have likewise been proposed as a solution to Reid's Paradox, concerning the disparity between predicted and observed rates of tree repopulation in Northern Britain after the last Ice Age (Clark et al. 1998). In our analysis, we demonstrated that geometric symmetrization can be used to accurately

describe the characteristics of an IDE with a Cauchy dispersal kernel, the prototypical example of a fat-tailed kernel. Supporting similar conclusions in Lutscher et al. (2005), Table 3 and Fig. 7 showed shifted kernels with higher kurtosis result in populations persisting at greater shift speeds, because there is a higher probability that some individuals will be able to disperse quite far, thus preserving the population. These results suggest that the effects of long-distance dispersal can indeed be captured by dispersal success approximations.

There are, of course, some caveats to our methods that are worth discussing. We used geometric symmetrization to quantify the asymptotic persistence of a population, but there are situations in which asymptotic behavior may be misleading. Transient population dynamics can sometimes imply extinction even when asymptotic dynamics suggest persistence (Caswell 2007). Caution is therefore appropriate when using geometric symmetrization to predict persistence.

There are many types of population models that we have not explored here in the context of geometric symmetrization. Integrodifference equations come in many different flavors, including ones that account for Allee effects (Wang et al. 2002), heterogeneous habitat (Van Kirk and Lewis 1997), and stage structure of populations (Harsch et al. 2014). Van Kirk and Lewis (1997) used the average dispersal success S to analyze an IDE on a network of patches and Lutscher and Lewis (2004) applied S to a stage-structured matrix population model; Reimer et al. (2016) recreated similar models for both of these scenarios and compared model performance to those using Reimer's modified $\widehat{S}$. We have not yet pursued these avenues with GS, but have no reason to believe that it would not continue to outperform S and $\widehat{S}$ in a shifting habitat or in the presence of advection. These models and others would benefit from further analysis.

Finally, our comparison of dispersal success characterizations is by no means complete, as there are many different ways to quantify dispersal success, and there are likely many as yet undiscovered methods that are worth exploring. Anticipating future efforts, we suggest that any meaningful definition of dispersal success should necessarily have three fundamental characteristics: a biological interpretation, a mathematical justification, and adherence to the principle of parsimony.

There are many examples in the literature of dispersal success being applied to ecological issues, but it is worthwhile to revisit these studies in the context of climate change. Fagan and Lutscher (2006) provide an eloquent argument for the usefulness of the average dispersal success in reserve network design, but Araújo et al. (2004) demonstrated that reserve selection methods are inadequate for ensuring the long-term persistence of species due to the effects of climate change. Hughes et al. (2015) demonstrated how dispersal success can model host-parasitoid interactions in a fragmented habitat, but there is considerable evidence to suggest that species interactions can be strongly influenced by climate change (Harrington et al. 1999; Hance et al. 2006). Cobbold et al. (2005) used the average dispersal success to quantify how parasitism affects the critical patch size of the forest tent caterpillar, but Potapov and Lewis (2004) found that the critical patch size of a species can increase as the rate of climate change increases. Clearly, the effects of climate change should not be ignored. Zhou and Kot (2011) demonstrated how climate change can be represented with a shifted dispersal kernel, and this framework continues to be developed and explored (Harsch et al. 2014; Phillips and Kot 2015; Bouhours and Lewis 2016).

Spatially explicit population models help elucidate the relationship between a population and its environment, and have proven to be quite useful for modeling biological processes such as growth and dispersal. Average dispersal success helps describe the aggregate population-level pattern of individual dispersal events, and geometric symmetrization enables us to describe the aggregate effects of asymmetric dispersal with a much greater degree of confidence in the approximations than other currently known methods. Moving forward, we heartily encourage using this method to incorporate asymmetric dispersal processes into spatially explicit population models.

Acknowledgements The author would like to thank Mark Kot for providing helpful feedback, guidance, and funding, and express gratitude to the reviewers for their helpful suggestions, especially Frithjof Lutscher and Mark Lewis. This material is based on work supported by the National Science Foundation under Grant No. DMS-1308365.

References

Alpin YA, Merikoski J (2010) A simple proof for the inequality between the Perron root of a nonnegative matrix and that of its geometric symmetrization. Lobachevskii J Math 31(3):222–223

Araújo MB, Cabeza M, Thuiller W, Hannah L, Williams PH (2004) Would climate change drive species out of reserves? An assessment of existing reserve-selection methods. Glob Chang Biol 10(9):1618–1626

Austerlitz F, Dutech C, Smouse P, Davis F, Sork V (2007) Estimating anisotropic pollen dispersal: a case study in Quercus lobata. Heredity 99(2):193–204

Baskett ML, Weitz JS, Levin SA (2007) The evolution of dispersal in reserve networks. Am Nat 170(1):59–78

Beverton RJ, Holt SJ (1957) On the dynamics of exploited fish populations. Fish Investig Series II 19:1–533

Bouhours J, Lewis MA (2016) Climate change and integrodifference equations in a stochastic environment. Bull Math Biol 78(9):1866–1903

Byers JE, Pringle JM (2006) Going against the flow: retention, range limits and invasions in advective environments. Mar Ecol Prog Ser 313:27–41

Caswell H (2001) Matrix population models, 2nd Edition. Sinauer, Sunderland
Caswell H (2007) Sensitivity analysis of transient population dynamics. Ecol Lett 10(1):1–15
Chen IC, Hill JK, Ohlemüller R, Roy DB, Thomas CD (2011) Rapid range shifts of species associated with high levels of climate warming. Science 333(6045):1024–1026
Clark JS, Fastie C, Hurtt G, Jackson ST, Johnson C, King GA, Lewis M, Lynch J, Pacala S, Prentice C et al (1998) Reid's paradox of rapid plant migration dispersal theory and interpretation of paleoecological records. BioScience 48(1):13–24
Clark JS, Silman M, Kern R, Macklin E, HilleRisLambers J (1999) Seed dispersal near and far: patterns across temperate and tropical forests. Ecology 80(5):1475–1494
Cobbold C, Lewis M, Lutscher F, Roland J (2005) How parasitism affects critical patch-size in a host–parasitoid model: application to the forest tent caterpillar. Theor Popul Biol 67(2):109–125
Fagan WF, Lutscher F (2006) Average dispersal success: linking home range, dispersal, and metapopulation dynamics to reserve design. Ecol Appl 16(2):820–828
Hance T, Van Baaren J, Vernon P, Boivin G (2006) Impact of extreme temperatures on parasitoids in a climate change perspective. Annu Rev Entomol 52(1):107
Harrington R, Woiwod I, Sparks T (1999) Climate change and trophic interactions. Trends Ecol Evol 14(4):146–150
Harsch MA, Zhou Y, HilleRisLambers J, Kot M (2014) Keeping pace with climate change: stage-structured moving-habitat models. Am Nat 184(1):25–37
Hughes JS, Cobbold CA, Haynes K, Dwyer G (2015) Effects of forest spatial structure on insect outbreaks: insights from a host-parasitoid model. Am Nat 185(5):E130–E152
Kolotilina LY (1993) Lower bounds for the Perron root of a nonnegative matrix. Linear Algebra Appl 180:133–151
Kot M, Phillips A (2015) Bounds for the critical speed of climate-driven moving-habitat models. Math Biosci 262:65–72
Kot M, Schaffer WM (1986) Discrete-time growth-dispersal models. Math Biosci 80(1):109–136
Kot M, Lewis MA, van den Driessche P (1996) Dispersal data and the spread of invading organisms. Ecology 77(7):2027–2042
Kot M, Medlock J, Reluga T, Walton DB (2004) Stochasticity, invasions, and branching random walks. Theor Popul Biol 66(3):175–184
Leslie PH (1945) On the use of matrices in certain population mathematics. Biometrika 33(3):183–212
Levin SA, Muller-Landau HC, Nathan R, Chave J (2003) The ecology and evolution of seed dispersal: a theoretical perspective. Ann Rev Ecol Evol Syst 34(1):575–604
Lutscher F, Lewis MA (2004) Spatially-explicit matrix models. J Math Biol 48(3):293–324
Lutscher F, Pachepsky E, Lewis MA (2005) The effect of dispersal patterns on stream populations. Siam Rev 47(4):749–772
Lutscher F, Nisbet RM, Pachepsky E (2010) Population persistence in the face of advection. Theor Ecol 3(4):271–284
May RM, Oster GF (1976) Bifurcations and dynamic complexity in simple ecological models. Am Nat 110(974):573–599
Nathan R, Muller-Landau HC (2000) Spatial patterns of seed dispersal, their determinants and consequences for recruitment. Trends Ecol Evol 15(7):278–285
Nathan R, Perry G, Cronin JT, Strand AE, Cain ML (2003) Methods for estimating long-distance dispersal. Oikos 103(2):261–273
Phillips A, Kot M (2015) Persistence in a two-dimensional moving-habitat model. Bull Math Biol 77(11):2125–2159
Potapov A, Lewis M (2004) Climate and competition: the effect of moving range boundaries on habitat invasibility. Bull Math Biol 66(5):975–1008
R Core Team (2017) R: a language and environment for statistical computing. R Foundation for Statistical Computing, Vienna. https://www.R-project.org/
Rahmandad H, Sterman J (2008) Heterogeneity and network structure in the dynamics of diffusion: comparing agent-based and differential equation models. Manag Sci 54(5):998–1014
Reimer JR, Bonsall MB, Maini PK (2016) Approximating the critical domain size of integrodifference equations. Bull Math Biol 78(1):72–109
Ricker WE (1954) Stock and recruitment. J Fish Board Canada 11(5):559–623
Rieux A, Soubeyrand S, Bonnot F, Klein EK, Ngando JE, Mehl A, Ravigne V, Carlier J, de Bellaire LdL (2014) Long-distance wind-dispersal of spores in a fungal plant pathogen: estimation of anisotropic dispersal kernels from an extensive field experiment. PLOS ONE 9(8):e103,225
Rodríguez MA (2010) A modeling framework for assessing long-distance dispersal and loss of connectivity in stream fish. In: Community ecology of stream fishes: concepts, approaches, and techniques, vol 73. American Fisheries Society, Symposium, Bethesda, pp 263–279
Rousseeuw PJ, Croux C (1993) Alternatives to the median absolute deviation. J Am Stat Assoc 88(424):1273–1283
Schloss CA, Nuñez TA, Lawler JJ (2012) Dispersal will limit ability of mammals to track climate change in the Western Hemisphere. Proc Natl Acad Sci 109(22):8606–8611
Schwenk AJ (1986) Tight bounds on the spectral radius of asymmetric nonnegative matrices. Linear Algebra Appl 75:257–265
Snyder RE (2003) How demographic stochasticity can slow biological invasions. Ecology 84(5):1333–1339
Trakhtenbrot A, Nathan R, Perry G, Richardson DM (2005) The importance of long-distance dispersal in biodiversity conservation. Divers Distrib 11(2):173–181
Van Kirk RW, Lewis MA (1997) Integrodifference models for persistence in fragmented habitats. Bull Math Biol 59(1):107–137
Vasilyeva O, Lutscher F, Lewis M (2016) Analysis of spread and persistence for stream insects with winged adult stages. J Math Biol 72(4):851–875
Veit RR, Lewis MA (1996) Dispersal, population growth, and the Allee effect: dynamics of the house finch invasion of eastern North America. Am Nat 148(2):255–274
Vuilleumier S, Possingham HP (2006) Does colonization asymmetry matter in metapopulations? Proc R Soc London B: Biol Sci 273(1594):1637–1642
Wang MH, Kot M, Neubert MG (2002) Integrodifference equations, Allee effects, and invasions. J Math Biol 44(2):150–168
Werth S, Wagner HH, Gugerli F, Holderegger R, Csencsics D, Kalwij JM, Scheidegger C (2006) Quantifying dispersal and establishment limitation in a population of an epiphytic lichen. Ecology 87(8):2037–2046
Willson M (1993) Dispersal mode, seed shadows, and colonization patterns. Vegetatio 107/108: 261–280
Willson MF, Traveset A (2000) The ecology of seed dispersal. Seeds: Ecol Regen Plant Commun 2:85–110
Zabreyko P, Koshelev A, Krasnoselskii M, Mikhlin S, Rakovshchik L, Stetsenko VY (2013) Integral equations: a reference text. Springer, Berlin
Zhou Y, Kot M (2011) Discrete-time growth-dispersal models with shifting species ranges. Theor Ecol 4(1):13–25